Published in final edited form as:
J Bionic Eng. 2011 June 10; 8(2): 114–121. doi:10.1016/S1672-6529(11)60017-6.

Biomimetic Precipitation of Uniaxially Grown Calcium Phosphate Crystals from Full-Length Human Amelogenin Sols

Vuk Uskoković[1], **Wu Li**[2], and **Stefan Habelitz**[1]

[1]Division of Biomaterials and Bioengineering, Department of Preventive and Restorative Dental Sciences, University of California, 707 Parnassus Avenue, San Francisco, CA 94143, USA

[2]Department of Orofacial Sciences, University of California, 513 Parnassus Avenue, San Francisco, CA 94143, USA

Abstract

Human dental enamel forms over a period of 2 – 4 years by substituting the enamel matrix, a protein gel mostly composed of a single protein, amelogenin with fibrous apatite nanocrystals. Self-assembly of a dense amelogenin matrix is presumed to direct the growth of apatite fibers and their organization into bundles that eventually comprise the mature enamel, the hardest tissue in the mammalian body. This work aims to establish the physicochemical and biochemical conditions for the synthesis of fibrous apatite crystals under the control of a recombinant full-length human amelogenin matrix in combination with a programmable titration system. The growth of apatite substrates was initiated from supersaturated calcium phosphate solutions in the presence of dispersed amelogenin assemblies. It was shown earlier and confirmed in this study that binding of amelogenin onto apatite surfaces presents the first step that leads to substrate-specific crystal growth. In this work, we report enhanced nucleation and growth under conditions at which amelogenin and apatite carry opposite charges and adsorption of the protein onto the apatite seeds is even more favored. Experiments at pH below the isoelectric point of amelogenin showed increased protein binding to apatite and at low Ca/P molar ratios resulted in a change in crystal morphology from plate-like to fibrous and rod-shaped. Concentrations of calcium and phosphate ions in the supernatant did not show drastic decreases throughout the titration period, indicating controlled precipitation from the protein suspension metastable with respect to calcium phosphate. It is argued that ameloblasts in the developing enamel may vary the density of the protein matrix at the nano scale by varying local pH, and thus control the interaction between the mineral and protein phases. The biomimetic experimental setting applied in this study has thus proven as convenient for gaining insight into the fundamental nature of the process of amelogenesis.

Keywords

Enamel; Amelogenin; Biomineralization; Apatite; Biomimetics

Introduction

Mimicking the formation of tooth enamel, the hardest tissue in the mammalian body, under *in vitro* conditions has the potential of delivering important fundamental insights into the physicochemical mechanism of this morphogenetic process [1]. These fundamental findings

Stefan Habelitz, PhD, MS Associate Professor in Residence Department of Preventive and Restorative Dental Sciences Division of Biomaterials and Bioengineering Tel: 415/514-0818 Fax: 415/476-0858 stefanhabelitz@ucsf.edu.

in turn have the prospect of resulting in advanced non-invasive treatments for remineralization of enamel in the clinical setting. In our previous study, we provided experimentally supported arguments that speak in favor of the capacity of amelogenin to promote nucleation and growth of calcium phosphate from lowly supersaturated solutions with respect to apatite[2]. These arguments were in agreement with the results of other similar studies [3,4,5]. Amelogenin assemblies are thus hypothesized not to act as inhibitors of the growth of apatite, but as bridges or channels that selectively deliver Ca^{2+} and PO_4^{3-} ions or amorphous units assembled on the surface of the protein from the solution onto the surface of the growing crystals[2]. These findings fit even earlier reports which claimed that adsorption of amelogenin onto the exposed crystalline faces of the seed crystals presents the first step for a controlled, substrate-specific growth to take place[6,7]. These results were obtained at physiological pH conditions, under which both amelogenin particles and apatite surfaces were negatively charged. The approach described in this work is based on the assumption that oppositely charged amelogenin and apatite surfaces might promote a more intensive electrostatic attraction and the physical drive for adsorption and the subsequent substrate-specific crystal growth. In our previous dynamic light scattering study we assessed pH conditions at which charge reversal for these two species occur[8]. A pH of 6.5 was selected for the purpose of this study because: (a) the protein and the mineral are oppositely charged at this pH[8]; and (b) the mildly acidic pH range has a physiological meaning since the developing enamel matrix is known to exhibit pH modulations in the range of 6.2 – 7.6[9].

A primary aim of the biomimetic setting of the experimental system applied hereby is to produce apatite crystals that resemble the morphology of enamel crystallites (Fig.1). Through such accomplishments fundamental understanding of the role of amelogenins in enamel mineralization could be advanced. A biomimetic methodology, such as the one applied in this study, has the prospect of leading to both practical and fundamental insights. In addition, amelogenesis may be seen as a convenient model for the study of interactions between protein and mineral phases relevant for biomineralization processes in general.

Experimental

The programmable titration experimental setting applied in this study was modified from a previous one[1] and previously reported[2]. The programmed titration was performed with 1 ml burettes, using a Titrino 751 GDP titration device in combination with a Dosimat 755 (*Brinkmann-Metrohm*) controlled by computer software (*Tiamo 1.2, Brinkmann-Methrohm*). The basic procedure was as follows. The reaction suspension comprising 5 ml of 0.4 mg/ml of full-length recombinant amelogenin protein (rH174), 20 mM Bis-Tris/HCl buffer, different concentrations of KH_2PO_4 and $CaCl_2$, and 0.02 % NaN_3 (introduced to the system in the given sequence) at pH 6.50 +− 0.01 was prepared in a glass vessel, which was kept at 37 °C via a circulating water bath (Fig.2). The two buffered titrant solutions (20 mM Bis-Tris/HCl, pH 6.50 +− 0.02) comprising the separate precursor ions ($CaCl_2$ and KH_2PO_4) and the electrolyte (142 $mmoll^{-1}$ KCl) up to the level of the physiological ionic strength were then continuously introduced into the reaction vessel at a controlled rate of 84 nl/min, i.e., 1.2 ml/day, cumulatively, throughout a 7-day period of time. The initial and titrant calcium and phosphate concentrations, as well as the titration rates and pH were modified in different experiments with the purpose of investigating the effects of different variables. Table 1 shows different ionic concentrations used. The crystal growth was initiated on polished glass ceramic substrates comprising embedded fluoroapatite (FAP) crystals with surface-exposed (001) faces[10]. A single substrate was sampled out each day and evaluated for the crystal growth properties using Atomic Force Microscopy (AFM, *Nanoscope III, Digital Instruments*) and Scanning Electron Microscopy (*SEM, DS130C, Topcon*). Tapping-mode AFM was applied using Si-tips with a radius of about 5 nm (*Supersharp,*

Nanosensors, Neuchatel, Switzerland). Full-length recombinant human amelogenin (rH174) was previously synthesized via expression in BL21(DE3) plysS *Escherichia Coli*[11,12]. The concentration of Ca^{2+} and $H_xPO_4^{x-3}$ in the reaction sol was followed using Inductively Coupled Plasma Optical Emission Spectrometry (ICP-OES, *Perkin Elmer, 5300 DV*).

The degrees of saturation (DS) at different reaction times were calculated using an algorithm based on Debye-Hückel equation[13], while taking into account the solvent evaporation rate at ca. 1 ml/day:

$$DS = pK_{sp} - pQ \quad \text{(Eq.1)}$$

$$Q = \left\{Ca^{2+}\right\}^5 \left\{PO_4^{3-}\right\}^3 \{OH^-\} \quad \text{(Eq.2)}$$

Q is the ionic activity product of the solution, and K_{sp} is the solubility product of hydroxyapatite ($Ca_5(PO_4)_3OH$, HAP), the negative logarithm of which was taken as equal to 58.65. Activity coefficients were calculated through $\log\gamma = -Az_i^2I^{1/2}$, where z_i is the charge number of ion species i, I is the ionic strength of the solution, and A is the constant depending on the dielectric constant of the solution, temperature and Debye screening length.

Results

Following immersion of FAP/glass substrates into rH174 sols, an adsorption of rH174 particles onto the substrates takes place. Fig.2 shows AFM images of rH174 deposits forming on the FAP/glass substrates at pHs 6.5 and 7.4. Whereas monodisperse nanosized particles with circa 20 – 40 nanometers in size adsorb at pH 7.4 (Fig.2a), uniform layers of the protein are formed at pH 6.5 (Fig.2d). As the titration time is increased, the nanospherical particles at pH 7.4 (Fig.2a) successively transform into protofibrous (Fig.2b) and fibrous assemblies (Fig.2c). SEM images shown in Fig.3 have confirmed this observation.

During the first 20 h of the titration time, the reaction suspension changed its appearance from turbid to only slightly opaque, indicating aggregation of the unstably dispersed microsized and polydisperse rH174 particles. In case of experiments carried out at pH 7.4, the stability of rH714 was markedly more pronounced. Consequently, a less drastic increase in the transparency of the mixture caused by colloidal destabilization was observed during the 7-day titration time. Already after 1 ml of titration at pH 6.5, the samples were covered with the precipitate. Unlike in the case of precipitation at pH 7.4 when the thickness of the precipitate reached 50 μm after 7 days of titration, markedly thicker deposits, on the millimeter scale, were obtained, although less evenly distributed, covering the substrate surface in steps. Elongated, centimeter sized particles were also formed in the solution and were observed as precipitated around the FAP substrates. Fig.3 shows different morphologies of the calcium phosphate precipitate formed upon precipitation from system III at pH 7.4 (Fig.4a) and system I at pH 6.5 (Fig.4b-d) using the identical DS of the titrant solutions (DS = 13.7 for the two combined titrants with respect to apatite). Whereas agglomerates of plate-shaped particles were obtained at pH 7.4, precipitation at pH 6.5 resulted in elongated, rod-shaped and fibrous calcium phosphate crystallites. Raman spectroscopic analysis has confirmed the presence of apatite in the precipitates (not shown here). The peak detected at 964.3 cm^{-1} and the absence of that at 1080 cm^{-1} suggested the

presence of non-carbonated apatite. Also, EDX analysis has confirmed the presence of calcium and phosphorus in all of the structures observed under SEM (Fig.5a).

When titration was carried out in the absence of rH174, no substrate-specific crystal growth was observed. Whereas the samples were fully covered with layers of uniaxially or biaxially grown particles when titration of rH174 sols was performed (Figs.4-5), exclusion of rH174 from the reaction mixture resulted in negligible formation of crystals on the substrate surface. AFM and SEM images of FAP/glass substrates after 9.3 ml of titration (Fig.6), showing the initial FAP crystals grown only up to ~ 100 nm in height, have demonstrated this. Calcium concentration in the supernatant for the control sample has shown a steady increase with only a late drop that indicated the onset of precipitation (Fig.7a). However, since no precipitate was observed as forming on the substrate surface, FAP/glass substrates may have only acted as a nucleation surface, from which the forming nuclei were detaching and dispersing in the solution in the absence of the protein layers. Phosphate concentration was kept at the constant level (Fig.7a), also indicating minimal precipitation of calcium phosphate in the early stages of the process. In contrast, the rH174-containing experiment (Fig.7b) has shown a less steep increase in calcium levels as well as a gradual drop in the concentration of phosphate, with no sudden drops thereof, indicating controlled precipitation of ions throughout the titration period.

Discussion

The comparison between the control, rH174-free titration experiments with those carried out on rH174 sols has shown that adsorption of amelogenin onto the crystal growth substrates presents the first step prior to their surface growth, and has thus confirmed our previous findings observed at pH 7.4 [7,2]. In the absence of deposition of amelogenin onto the substrate surface, no substrate-specific growth is observed. At pH 7.4 the protein adsorption proceeds at a significantly lower rate compared to that occurring at pH 6.5. One of the reasons is in a lesser stability that colloidal nanospheres of amelogenin exhibit in aqueous suspension in the pH range 4.5 – 7.0, as demonstrated by our previously reported analyses[14]. Amelogenin nanospheres tend to aggregate in this pH range and their precipitation thus becomes favored. In contrast, at pH < 4.5 and pH > 7, amelogenin nanospheres are well dispersed and stable in suspension. In the vicinity of the isoelectric point of amelogenin (~ 6.8), the repulsive force between individual amelogenin nanospheres is minimal and their reversible aggregation occurs, resulting in destabilization and gradual phase segregation of the resulting suspension.

As indicated by our former zeta-potential studies, rH174 and FAP seeds also carry opposite charges at pH 6.5, which has been shown to present an additional factor that promotes adsorption of rH174 onto FAP[8]. This more intensive adsorption may be a factor that leads to a more extensive and earlier crystal growth at pH 6.5 compared to pH 7.4. The greatly enhanced crystal growth effect is presumed to be owing to a more efficient adsorption of the protein assemblies onto the crystalline surface. Thus, even decreasing DS of the combined titrant solution by more than four units (13.6 for system I → 9.3 for system III) yielded equally extensive amounts of crystal growth at pH 6.5. Unlike in the experiments starting with DS < 0 and carried out at pH 7.4, in those taking place at pH 6.5 high initial levels of Ca^{2+} (system II) produced earlier extensive precipitation compared to those performed at high initial levels of $H_xPO_4^{x-3}$ (system III). Whereas the former system exhibited extensive crystal growth after ~ 1.3 ml of titration, 2.5 – 3.8 ml of the titration volume was required to reach the same level of crystal growth in the latter. This may be explained by the fact that calcium phosphate solutions at Ca/P molar ratios > 1 have a larger number of phases that may possibly form. Hence, under the conditions used in our experiments, after 1 ml of titration system II becomes supersaturated with respect to three calcium phosphate phases

(hydroxyapatite, octacalcium phosphate and β-tricalcium phosphate), whereas system III becomes supersaturated only with respect to hydroxyapatite, although at a significantly lower level too (DS = 4.9 compared to 7.3 for system II).

Owing to an attraction between oppositely charged rH174 (+) and FAP (−) at pH 6.5, even samples analyzed after the reaction times prior to the onset of precipitation show evidence of a protein layer adsorbed on the apatite substrates. Owing to the non-discrete nature of amelogenin assemblies, AFM analyses of the sample surfaces even after the earliest reaction times (0.5 – 1 ml of titration volume) were made difficult and did not yield significant information on the fine structure of these uniform protein layers. SEM analysis of the morphologies of the grown crystals indicated the presence of needle-shaped apatite crystallites (Fig.4c-d), particularly resembling the elongated apatite crystals of enamel (Fig. 1). In general, whereas precipitation at pH 6.5 in system I yielded elongated, rod-shaped (Fig.4c-d) and fibrous (Fig.4b) calcium phosphate particles, those carried out at pH 7.4 led to a more pronounced plate-shaped character thereof (Fig.4a).

Rod-shaped particles were also obtained only in system I, which had a lower Ca/P molar ratio compared to systems II-III. It was reported earlier that the fluid of the developing enamel contains calcium concentrations of around 0.5 mM, while the concentration of phosphates averages at around 3.9 mM[15]. The Ca/P molar ratio of the developing enamel matrix is at 0.2 markedly lower than that of the Ca/P molar ratio of pure hydroxyapatite stoichiometry: 1.667. After 1 ml of titration in system I, the Ca/P molar ratio is at 0.26 close to the one of the developing enamel fluid. It is possible that a comparatively low Ca/P molar ratio is important for promotion of the uniaxial growth of the apatite particles. The elongation of precipitated particles at high anionic contents fits the previous observations of the aspect ratio of ceramic nanorods as directly proportional to anionic concentrations[16].

As our previous study has pointed out that pH 7.4 lies close to the boundary of the pH zone wherein amelogenin nanospheres aggregate forming microsized entities [14], ameloblasts may be able to vary the density of the protein matrix at the nano scale by varying local pH, particularly since it is known that pH of the enamel matrix exhibits modulations in the range of 6.2 – 7.6 [9]. Ameloblasts are able to adjust the pH of the enamel fluid, and their rhythmical change from smooth to ruffled ended cells is accompanied by a local pH change in the surrounding enamel fluid from nearly physiological (7.2 – 7.4) to slightly acidic (6.1 – 6.8) [17]. Furthermore, as ζ-potential of hydroxyapatite is negative in the entire pH range of its stability [8], whereas rH174 exhibits isoelectric point at 6.8 +− 0.2 [14], subtle pH changes can be applied to modify the intensity of the attraction between the protein and the mineral phase. Thus, at pH < 6.8 +− 0.2, the protein and the mineral surfaces would be oppositely charged, whereas at pH > 6.8 +− 0.2, they would carry the same, negative charge. With shifting the surface charge of the amelogenins and thereby modifying their propensities for assembly and interaction with the growing mineral phase, ameloblasts may have a crucial role in guiding the process of amelogenesis. The underlying Tomes' process may be furthermore crucial in aligning the apatite fibers along the same direction and preventing their random tilting in space. Further studies will tend to elucidate these effects in more detail.

Conclusions

This work has fallen into the scope of our study that aims to establish the physicochemical and biochemical conditions for the synthesis of fibrous apatite crystals under the control of a recombinant full-length human amelogenin matrix in combination with a programmable titration system. The growth of apatite substrates was initiated from supersaturated calcium phosphate solutions in the presence of dispersed amelogenin assemblies. The study has

confirmed the previous findings that binding of amelogenin onto apatite surface presents the first step that leads to substrate-specific crystal growth. It has been shown that enhanced nucleation and growth result from conditions under which amelogenin and apatite carry opposite charges and adsorption of the protein onto the apatite seeds is favored. Experiments at pH below the isoelectric point of amelogenin showed increased protein adsorption onto apatite seeds and at low Ca/P molar ratios resulted in a change in crystal morphology from plate-like to fibrous and rod-shaped. Concentrations of calcium and phosphate ions in the supernatant did not show drastic decreases throughout the titration period, indicating controlled precipitation from the protein suspension metastable with respect to calcium phosphate. It is argued that ameloblasts in the developing enamel may vary the density of the protein matrix at the nanoscale by varying local pH, and thus control the interaction between the mineral and protein phases. The biomimetic experimental setting applied in this study has thus proven as convenient for gaining insight into the fundamental nature of the process of amelogenesis.

Acknowledgments

Presented were the results of a study supported by NIH/NIDCR grants R01-DE017529 and R01-DE017529-S2. The authors would like to thank Dr. Christian Russel (FSU Jena, Germany) for providing the glass-ceramic substrates, Anora Burwell for the assistance with ICP analyses, and Li Zhu, Joseph Mendoza and Feroz Khan (UCSF) for the synthesis of rH174.

References

[1]. Uskoković V, Kim M, Li W, Habelitz S. Enzymatic processing of amelogenin during continuous crystallization of apatite. Journal of Materials Research. 2008; 23:3184–3195. [PubMed: 19177182]

[2]. Uskokovic V. Amelogenin as a Promoter of Nucleation and Crystal Growth of Apatite. Journal of Crystal Growth. 2011 in press.

[3]. Wang L, Guan X, Du C, Moradian-Oldak J, Nancollas G. Amelogenin Promotes the Formation of Elongated Apatite Microstructures in a Controlled Crystallization System. J. Phys. Chem. C. 2007; 111:6398–6404.

[4]. Wang Mimicking the Self-Organized Microstructure of Tooth Enamel. Journal of Physical Chemistry C. 2008; 112

[5]. Tarasevich B, et al. The nucleation and growth of calcium phosphate by amelogenin. Journal of Crystal Growth. 2007; 304:407–415. [PubMed: 19079557]

[6]. Habelitz S, DenBesten P, Marshall S, Marshall G, Li W. Amelogenin control over apatite crystal growth is affected by the pH and degree of ionic saturation. Orthod Craniofac Res. 2005; 8:232–238. [PubMed: 16238603]

[7]. Habelitz S, et al. Amelogenin-guided Crystal Growth on Fluoroapatite Glass-ceramics. Journal of Dental Research. 2004; 83:698–702. [PubMed: 15329375]

[8]. Uskokovic V. Dynamic Light Scattering and Zeta Potential of Hydroxyapatite and Amelogenin Nanoparticles. Archives of Oral Biology. 2010

[9]. Sasaki S, Takagi T, Suzuki M. Cyclical changes in pH in bovine developing enamel as sequential bands. Archives of Oral Biology. 1991; 36:227–231. [PubMed: 1877895]

[10]. Moisescu C. Oriented fluoroapatite glass-ceramics. Journal of Non-Crystalline Solids. 1999; 248:176–182.

[11]. Li W. X-linked amelogenesis imperfecta may result from decreased formation of tyrosine rich amelogenin peptide (TRAP). Archives of Oral Biology. 2003; 48:177–183. [PubMed: 12648554]

[12]. Zhu L, et al. Comparative properties of recombinant human and bovine matrix metalloproteinase-20. Archives of Oral Biology. 2008; 53:785–790. [PubMed: 18336793]

[13]. Larsen, MJ. Ion Products and Solubility of Calcium Phosphates. Royal Dental College; 2001.

[14]. Uskokovic V, et al. Zeta-potential and Particle Size Analysis of Human Amelogenins. Journal of Dental Research. 2009; 89:149–153. [PubMed: 20040742]

[15]. Aoba T, Moreno EC. The enamel fluid in the early secretory stage of porcine amelogenesis: Chemical composition and saturation with respect to enamel mineral. Calcif Tissue Int. 1987; 41:86–94. [PubMed: 3115550]

[16]. Filankembo A, Giorgio S, Lisiecki I, Pileni MP. Is the Anion the Major Parameter in the Shape Control of Nanocrystals? J. Phys. Chem. B. 2003; 107:7492–7500.

[17]. Smith C. Cellular and Chemical Events During Enamel Maturation. Critical Reviews in Oral Biology & Medicine. 1998; 9:128–161. [PubMed: 9603233]

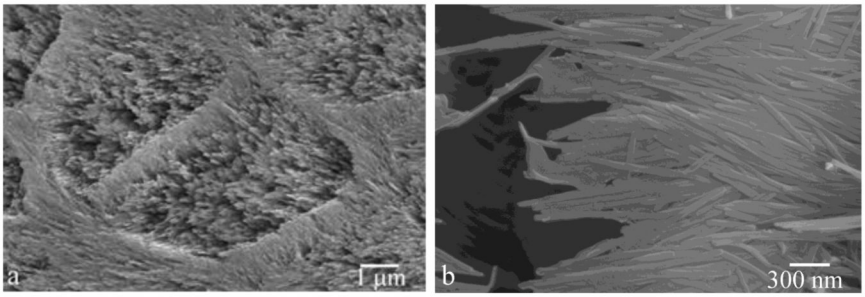

Fig.1.
SEM images of natural tooth enamel morphologies: individual apatite nanofibers (a) and their organization into keyhole-shaped bundles called enamel rods (b).

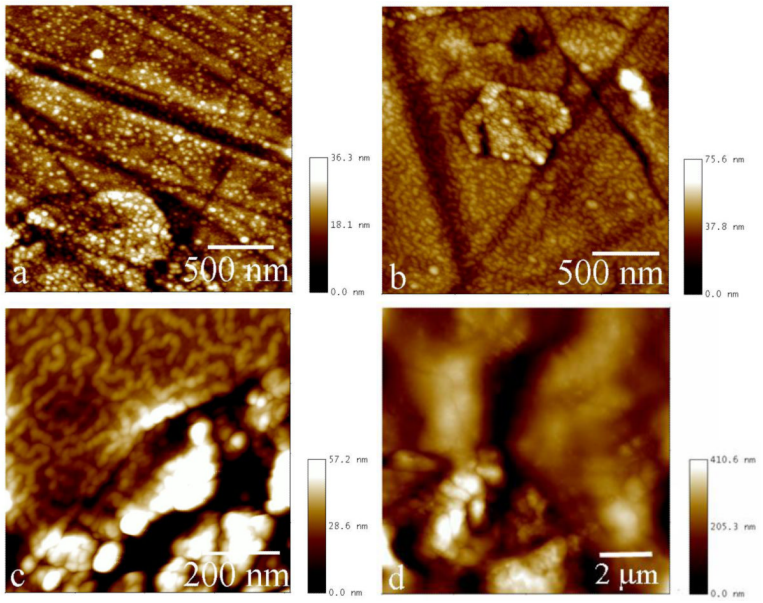

Fig.2.

FAP/glass substrates with rH174 deposits formed in system III run at pH 7.4 after 1 ml (a), 1.6 ml (b), and 2.5 ml (c) of titration volume, and at pH 6.5 after 2.5 ml of titration volume (d).

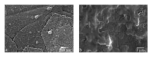

Fig.3.
SEM images of FAP/glass substrates with rH174 deposits formed at pH 7.4 (a) and pH 6.5 (b) after 2.5 ml of titration volume.

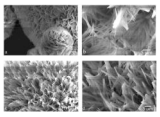

Fig.4.
SEM micrographs of apatite morphologies obtained in system III run at pH 7.4 (a and c), and in system I run at pH 6.5 (b-d), after titration volume of 9.5 ml.

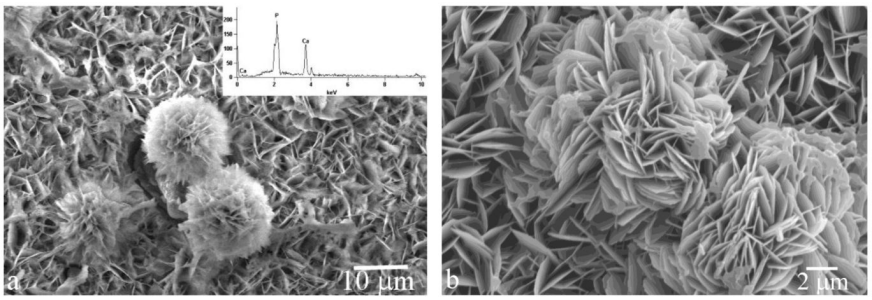

Fig.5.
SEM micrographs of apatite morphologies obtained in systems II (a) and III (b), after the titration volumes of 1.3 (a) and 4 ml (b).

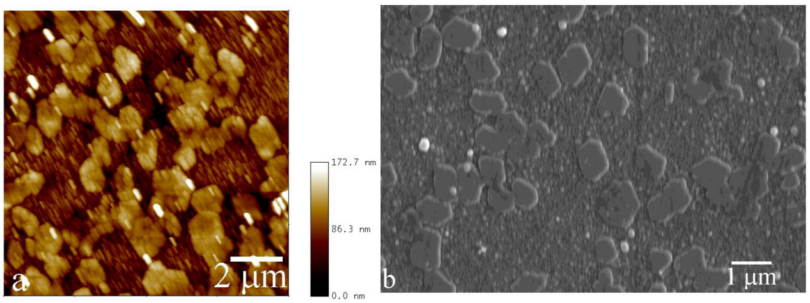

Fig.6.
AFM (a) and SEM (b) images of FAP/glass substrates sampled out from a control, protein-free system I after 9.3 ml of titration.

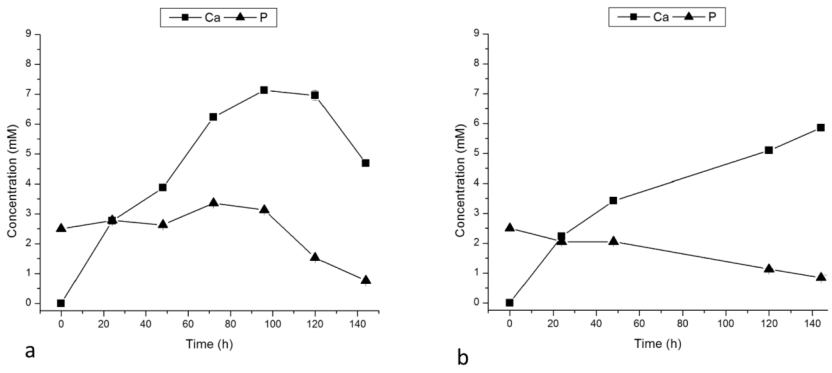

Fig.7.

Calcium and phosphate concentrations in the supernatants of system III after different titration times in control, rH174-free (a) and rH174-containing system I (b).

Table 1

Different ionic concentrations in the initial reaction systems and in the titrant solutions for different apatite crystallization experiments.

System	Initial [Ca^{2+}] (mM)	Initial [$H_xPO_4^{x-3}$] (mM)	Titrant [Ca^{2+}] (mM)	Titrant [$H_xPO_4^{x-3}$] (mM)
I	0	10	16	10
II	4.1	0	4.1	2.5
III	0	2.5	4.1	2.5